International Journal of Engineering Science 134 (2019) 31–46

Contents lists available at ScienceDirect

International Journal of Engineering Science

journal homepage: www.elsevier.com/locate/ijengsci

Theoretical framework for percolation threshold, tortuosity and transport properties of porous materials containing 3D non-spherical pores

Wenxiang Xu[a,*], Yang Jiao[b]

[a] Institute of Structures and Materials Mechanics, College of Mechanics and Materials, Hohai University, Nanjing 211100, China
[b] Materials Science and Engineering, Arizona State University, Tempe, AZ 85287, USA

ARTICLE INFO

Article history:
Received 24 August 2018
Revised 17 October 2018
Accepted 17 October 2018
Available online 25 October 2018

Keywords:
Porous materials
Non-spherical pore
Percolation
Tortuosity
Transport properties

ABSTRACT

Understanding the effects of porous network characteristics including the percolation and tortuosity on transport properties of porous materials is of great importance for the design and optimization of such materials, e.g., for superior resistance to degradation due to the transfer of corrosive fluids. Meanwhile, the percolation and tortuosity of porous networks are strongly affected by the geometrical shape of pores. In this work, we devise a generic theoretical framework for the accurate predictions of the percolation threshold and tortuosity of porous networks and a variety of transport properties of two-phase porous materials composed of three-dimensional (3D) interpenetrating non-spherical pores randomly distributed in a homogeneous solid matrix. Our framework contains three major components: (1) a coupled scheme of Monte Carlo simulations and a rigorous excluded-volume percolation model for determining of the percolation threshold of porous networks; (2) a continuum percolation-based tortuosity model (CPTM) for deriving the geometrical tortuosity of porous networks near the percolation threshold and above; and (3) a continuum percolation-based generalized effective medium theory (CP-GEMT) for predicting various effective transport properties including the effective diffusivity, permeability, electrical and thermal conductivity of porous materials over the entire range of porosities. The theoretical framework yields accurate predictions of the percolation threshold, tortuosity and various effective transport properties, which are verified and validated using extensive experimental, numerical and analytical data for a wide spectrum of different porous materials reported in literature. Our framework is readily applicable to other non-spherical percolating networks composed of interpenetrating discrete objects like cracks, particles, interfaces, capsules and tunneling networks though 3D spherocylindrical porous networks are used as an introductory example in this work. Finally, we utilize the framework to explore the influences of the pore geometrical configurations on the tortuosity and effective diffusivity of porous materials. The results shed light on the intrinsic and complex interplay of components, structures and transport properties in porous materials, which in turn can provide novel insights for understanding degradation of porous materials in practical applications.

* Correspondence author at: Institute of Materials and Structures Mechanics, College of Mechanics and Materials, Hohai University, Nanjing 211100, China.
E-mail addresses: xwxfat@gmail.com (W. Xu), yang.jiao.2@asu.edu (Y. Jiao).

https://doi.org/10.1016/j.ijengsci.2018.10.004
0020-7225/

1. Introduction

Porous materials are ubiquitous in areas of geoscience and advanced and engineering materials, such as soil, rock, polymer, ceramic, concrete and other porous composites, to name but a few. It is well known that porous networks are the main transport "channels" for active media (e.g., contaminant, iron, carbon dioxide, heat/electron/fluid, etc.) in porous materials. Also, the transport velocity and path of active media are significantly dependent on porous network characteristics including the percolation (connectivity) and tortuosity (Hermann & Elsner, 2014; Sevostianov, Trofimov, Merodio, Penta, & Rodriguez-Ramos, 2017; Sevostianova, Leinauer, & Sevostianov, 2010). Specifically, the percolation of porous networks triggers the dramatic change of transport properties of porous materials in the vicinity of the percolation threshold (Hunt & Sahimi, 2017; Nan, Shen, & Ma, 2010; Sahimi, 2003; Torquato, 2002), which is generally characterized by the critical porosity. Such porous structural configurations and physico-mechanical properties are seriously impacted by the geometrical shape of pores (Giraud, Nguyen, & Grgic, 2012; Markov, Mousatov, Kazatchenko, & Markova, 2013; Sevostianov & Giraud, 2013; Sevostianov, Chen, Giraud, & Grgic, 2016; Trofimov, Abaimov, Akhatov, & Sevostianov, 2018a, 2018b; Xu, Sun, Chen, & Chen, 2018c). Therefore, understanding the effect of pore shape on the percolation and tortuosity of porous networks and rigorously incorporating such structural characteristics into the prediction of transport properties of porous materials is of great significance for illuminating the intrinsic and complex interplay of components, structures and transport properties in porous materials. However, it is a formidable challenge to practically capture such intrinsic interactions through laboratory investigations.

Percolation of porous networks describes the interconnectivity of pores and the emergence of pore-spanning cluster in porous materials. Its measurement includes experimental test, and theoretical and numerical evaluations. Mercury intrusion porosimetry (MIP) test as the most common experimental measurement on porous structures, assumes the geometry of pores to be the uniform spherocylindrical shape, through which the percolation threshold is empirically evaluated based on the portrayed pore size distribution curve (Winslow, Cohen, Bentz, Snyder, & Garboczi, 1994). Diamond (2000) yet reviewed that MIP is an inappropriate method for the measurement of porous structures in porous materials. Through theoretical and numerical investigations on percolation, it can be traced to the pioneering work of Broadbent and Hammersley (1957) who studied for the first time the percolation threshold using a lattice model for the fluid flow in a random medium. Over nearly six decades, lattice percolation classified into two types of bond percolation and site percolation has been deeply researched from various scholars. An extensive list of references of the existing studies on lattice percolation can be found in the comprehensive review papers (Araújo, Grassberger, Kahng, Schrenk, & Ziff, 2014; Isichenko, 1992; Kirkpatrick, 1973; Stauffer & Aharony, 2003; Xu et al., 2018c). Nevertheless, regular lattice networks cannot illustrate the effect of geometrical shape of pores on the percolation threshold (Stauffer & Aharony, 2003; Torquato, 2002; Xu et al., 2018c).

Compared to lattice percolation, another percolation type, namely, continuum percolation possesses two remarkable merits to characterize the percolation of porous networks: discrete pores can be of any geometrical morphology to consist in a percolating cluster, and they are not restricted in fixed bonds or sites in a lattice network but are placed in arbitrary space. Strictly speaking, continuum percolation is the general of lattice percolation. Several investigations on continuum percolation of discrete pores represented by overlapping objects of different geometrical shapes have been implemented in three-dimensional (3D) space (Lin, Chen, & Xu, 2018; Mutiso, Sherrott, Li, & Winey, 2012; Rintoul & Torquato, 1997; Torquato & Jiao, 2012, 2013; Xu, Su, & Jiao, 2016b; Xu, Zhu, & Zhang, 2018e). Here, we focus on the spherocylindrical pores following the experimental assumptions (Diamond, 2000; Winslow et al., 1994). Although the continuum percolation of overlapping spherocylinders has received increasingly attention, including theoretical approximations based on the excluded-volume model (Balberg, Binenbaum, & Wagner, 1984) and Monte Carlo simulations (Mutisoet al., 2012; Schilling, Miller, & van der Schoot, 2015; Xu et al., 2016b), a general scheme for accurately determining the percolation threshold of anisotropic pores has not been systematically investigated.

On the other hand, the tortuosity is usually used to portray the tortuous path of active media transfer in porous materials (Xu, Jia, & Gong, 2018a), as shown in Fig. 1. In terms of the functionalities of the use of tortuosity in varies fields, it is roughly categorized into four types including the geometrical tortuosity, electrical tortuosity, diffusive tortuosity and hydraulic tortuosity (Clennell, 1997). As reviewed by Clennell (1997), the electrical tortuosity is delineated in accordance with the conduction of electrical current. The diffusive tortuosity is probed from temporal changes in concentration, and the hydraulic tortuosity is normally described geometrically. Therefore, these tortuosities illustrate different transport processes and possess individual physical meanings in porous materials. This study concentrates the geometrical tortuosity τ that is often defined as the ratio of the actual length (or the geometrical average length, $\langle L_a \rangle$, see Fig. 1) of flow path of fluids throughout pore space and the straight-line length L of a system size (Clennell, 1997; Ghanbarian, Hunt, Sahimi, Ewing, & Skinner, 2013; Yun, Yu, Zhang, & Huang, 2005, 2010).

$$\tau = \frac{\langle L_a \rangle}{L} \tag{1}$$

Apparently, τ is always larger than unit according to Eq. (1). However, it is not accessible to the task for the probe of actual length of flow path in practice, owing to the disordered nature of porous networks.

Numerical and theoretical explorations have been presented to evaluate tortuosity. For example, Yun and coworkers (2005, 2010) applied a simple geometrical approximation to statistically estimate the geometrical tortuosity of saturated porous media with rigid spherical and cylindrical particles. A similar research has also been manipulated for a rigid cubic

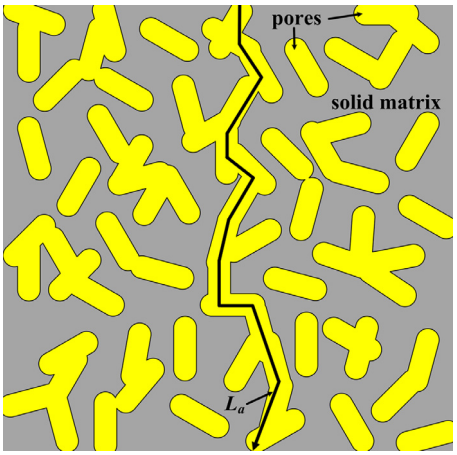

Fig. 1. Schematic view of the tortuous flow path of fluids in porous materials.

particle system (Tang, Sun, & Cheng, 2012). Alternatively, in the outstanding work from Sevostianov and Shrestha (2010), they presented two theoretical bounds for tortuosity respectively based on the Hashin–Shtrikman bound (Hashin & Shtrikman, 1962) and Beran bound (Beran, 1968) for conductivity, and even explicitly developed the bounds and closed-form cross-property connection for the effective conductivity and permeability governed by tortuosity values of porous and solid phases consisting in a two-phase porous material. As stated by Ghanbarian et al. (2013), when the porosity achieves the percolation threshold or above, a power-law in percolation theory may dominate the properties of porous media including the tortuosity and transport properties, irrespective of particle geometries in porous media. Indeed, numerous prominent studies (Hunt, 2004; Hunt & Sahimi, 2017; Nan et al., 2010; Xu et al., 2018a) have manifested the transport properties of porous materials near the percolation threshold (the critical porosity) follow a power-law, such as the famous Archie′s law (Hunt, 2004; Hunt & Sahimi, 2017). Accordingly, Ghanbarian et al. (2013) utilized the lattice percolation theory to predict the tortuosity of porous media, which is useful to link the tortuosity to the percolation threshold of pore space. However, such modeling works are missing the effect of pore shape on the tortuosity of porous networks near the percolation threshold and above. It is one of objectives of this work.

Over the past decades, significant efforts have been devoted to predicting the effects of characteristics of pore space on the effective properties of porous materials. Previous works in this area involved the application of effective medium theories including rigorous bounds (Torquato & Pham, 2004; Trofimov et al., 2018a; Xu, 2012), self-consistent scheme (SCS) and generalized SCS (Giraud et al., 2012; Pabst & Gregorová, 2014; Xu et al., 2014; 2016a), Mori–Tanaka method (Suvorov & Selvadurai, 2011; Trofimov, Markov, Abaimov, Akhatov, & Sevostianov, 2018b; Xu, Wu, Jiao, & Liu, 2017a, 2017b, 2018d), differential effective medium approximation (D-EMA) and generalized D-EMA (Markov et al., 2013; Xu et al., 2018b), generalized Maxwell model (Sevostianov & Giraud, 2013), etc. In these homogeneous schemes, porous materials are viewed as a two-phase composite composed of homogeneous matrix and impenetrable inclusions representing discrete pores or obstacles with various geometries like rigid spherical, superspherical, ellipsoidal or cylindrical inclusions, and even as a three-phase composite containing interphase between inclusions and matrix (Xu, Chen, Chen, & Jiang, 2014, 2016a, 2017a, 2017b, 2018d). A nonlinear scaling of transport properties with inclusion fraction is immediately yielded once the global connectivity of rigid inclusions occurs in porous materials. By this way, the critical porosity is empirically evaluated by identifying the abrupt change value on the derived nonlinear scaling curve (Giraud et al., 2012; Markov et al., 2013; Suvorov & Selvadurai, 2011; Xu, 2012; Xu et al., 2017a). However, the evaluated critical porosity may be not the precise percolation threshold, which will be discussed in this work (see Section 5.2). Moreover, they cannot predict the quantitative scheme of the percolation of interpenetrating anisotropic-shaped pores on the effective properties of porous materials. The fact that the evaluated percolation threshold using the effective medium theories were not in agreement with the percolation theory has been well documented (Xu et al., 2018a), due to the potential limitation for the applicability of effective medium theories in the dilute cases.

Alternatively, regarding porous materials with interpenetrating pores and solid matrix, McLachlan (1987) developed a generalized effective medium theory (GEMT) to bridge the percolation threshold of interpenetrating pores (or discrete inclusions) to the effective conductivity of porous materials with a broad range of porosity. Afterwards, GEMT has been extensively applied to investigate the effective transport properties of various porous media. For instance, Oh and Jiang (2004) employed GEMT to investigate the effective diffusivity of cement paste near the critical capillary porosity as an experimental fitting parameter. Brosseau (2002) evaluated the effective permittivity of two-phase particulate composites near the percolation threshold ($\phi_c = 1/3$) of interpenetrating spherical particles through GEMT. Recently, Ghanbarian and Daigle (2016) estimated the effective thermal conductivity of two-phase porous media by coupling GEMT with lattice percolation. Regardless of these important works in this area, results have not thrown much fresh light on the effect of the accurate percolation

threshold of interpenetrating anisotropic-shaped pores on the effective transport properties of porous materials (like the diffusivity, permeability, conductivity). It is another objective of the present work to address this lacuna.

In this study, porous materials at a microscopic level are regarded as two-phase composite media containing homogeneous solid matrix and porous networks composed of 3D interpenetrating anisotropic-shaped pores. We attempt to present a general scheme that integrates Monte Carlo simulations into the finite-size scaling scheme to determine the percolation threshold of anisotropic-shaped pores. It has been evidenced that the finite-size scaling analysis is a powerful means for the precise determination of percolation threshold in the infinite-size system. A continuum percolation-based tortuosity model (CPTM) is developed to derive the geometrical tortuosity of porous networks near the percolation threshold and above. Furthermore, a continuum percolation-based generalized effective medium theory (CP-GEMT) that incorporates the derived continuum percolation model into GEMT is proposed to predict the various effective transport properties of porous media. These continuum percolation-based models suggest a generic framework for precise predictions of the percolation threshold, tortuosity and effective properties of composite media containing non-spherical pores or objects (like cracks, particles, fibers, interfaces, capsules and tunneling networks), though the present anisotropic-shaped pores are considered as spherocylindrical objects following the experimental investigations.

The rest of this paper is organized as follows. Section 2 describes the continuum percolation of porous networks, where a rigorous excluded-volume percolation model is given and compared with numerical and experimental data. The continuum percolation-based tortuosity model (CPTM) is demonstrated in Section 3, where it is verified by comparing against experimental and numerical results reported in literature. Section 4 presents the continuum percolation-based generalized effective medium theory (CP-GEMT). Experimental measurements for various transport parameters like the diffusivity, gas permeability, electrical conductivity and thermal conductivity in different porous materials and other theoretical models are adopted to test the proposed CP-GEMT. Section 5 presents the sensitivity of the present CPTM and CP-GEMT to their parameters, such as the porosity, geometrical shape and transport-percolation exponent. Section 6 gives our conclusions and remarks.

2. Continuum percolation of porous networks

In the lattice percolation theory, a correlation length ξ that illustrates the mean distance between any two sites on the same cluster in an infinite-size system can be defined by (Stauffer & Aharony, 2003)

$$\xi \propto |p - p_c|^{-\nu}, \text{or} \xi = C|p - p_c|^{-\nu} \tag{2}$$

where p is the fraction of sites and p_c is the percolation threshold. ν is a critical correlation length exponent, which is thought to be a universal value only dependent on the space dimension (e.g., $\nu = 4/3$ in two-dimension (2D) and $\nu = 0.88$ in 3D) in lattice percolation (Hunt & Sahimi, 2017; Isichenko, 1992; Kirkpatrick, 1973; Stauffer & Aharony, 2003). C is a coefficient that is not universal. For example, Kapitulnik, Aharony, Deutscher, and Stauffer (1983) found $C = 0.85$ in units of the bond length. When $p > p_c$, ξ represents a length scale over which the macroscopic properties of the system are homogeneous; otherwise ξ describes the typical radii of clusters in the system. However, this definition is not suited to a precise determination of the percolation threshold of complex geometrical objects. As introduced in the preceding section, continuum percolation can address this gap and extrapolate from finite-size systems to the infinite-size system through the finite-size scaling analysis.

In the present continuum percolation, the percolation threshold is characterized by the critical porosity ϕ_c replacing p_c in lattice percolation. ϕ_c illustrates the critical state of emergence of a system-spanning cluster in the infinite-size limit, which is here called as the global percolation threshold. In practice, this limit state can be scaled by the extrapolation of the local percolation thresholds of finite-size systems, namely, the well-known finite-size scaling analysis, which have been broadly applied to lattice percolation (Kirkpatrick, 1973; Stauffer & Aharony, 2003), is given by

$$\Delta(L) \propto L^{-1/\nu}, \text{and} \phi_c(L) - \phi_c \propto L^{-1/\nu} \tag{3}$$

where $\phi_c(L)$ is the local percolation threshold of finite system of size L. $\Delta(L)$ characterizes the percolation transition width of finite-size system. Both quantities are size-dependence. Obviously, once $\phi_c(L)$ and $\Delta(L)$ are obtained, the global percolation threshold ϕ_c of infinite-size system can be estimated by the scaling relation of Eq. (3).

For deriving $\phi_c(L)$ and $\Delta(L)$, a useful way is to require the percolation probability P versus the porosity ϕ in a finite system of L, since the curve of P-ϕ has a sigmoidal shape and the values of $\phi_c(L)$ and $\Delta(L)$ can be approximated by using the error function of $P = \{1 + \text{erf}[(\phi - \phi_c(L))/\Delta(L)]\}/2$ (Lin et al., 2018; Rintoul & Torquato, 1997; Xu et al., 2016b) to fit the curve of P-ϕ. Accordingly, we start from the establishment of numerical realizations of two-phase porous materials through Monte Carlo simulations, aiming at obtaining the percolation probability $P(\phi, L)$. A numerical realization is generated by randomly placing interpenetrating anisotropic-shaped pores of a uniform size with the porosity ϕ into a cubic cell of size L with periodic boundary conditions (see Fig. 2). Note that positions and orientations of pores are totally uncorrelated and follow the Poisson distribution. Size-polydispersity of pores does not appear to influence the global percolation threshold in the infinite-size system (Mutisoet al., 2012; Torquato & Jiao, 2012, 2013; Xu et al., 2016b). The percolation probability P is defined as the ratio of the number of percolated realizations to the whole number of realizations. Towards this end, a percolating cluster in each realization is identified as the connective pathway of pores entirely wrapping the cubic cell from one boundary to another boundary by the “tree-burning” algorithm (Xu et al., 2016b). Fig. 3 presents the visualizations of

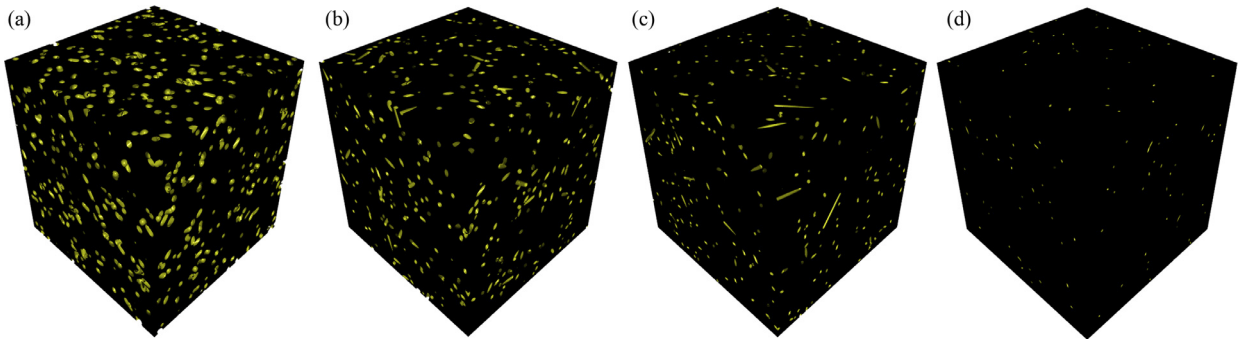

Fig. 2. Visualizations of two-phase porous materials as a finite-size cubic cell of $L=50$ with periodic boundary conditions consisting of homogeneous solid matrix (black parts) and interpenetrating spherocylindrical pores (yellow inclusions) with various α: (a) $\alpha=1$, (b) $\alpha=4$, (c) $\alpha=10$, and (d) $\alpha=50$. The size of spherocylindrical pores is specified to be $R_{eq}=1.0$, where R_{eq} is the equivalent radius as the size descriptor of anisotropic pores and its definition has been given by Xu et al. (2016b). (For interpretation of the references to colour in this figure legend, the reader is referred to the web version of this article.)

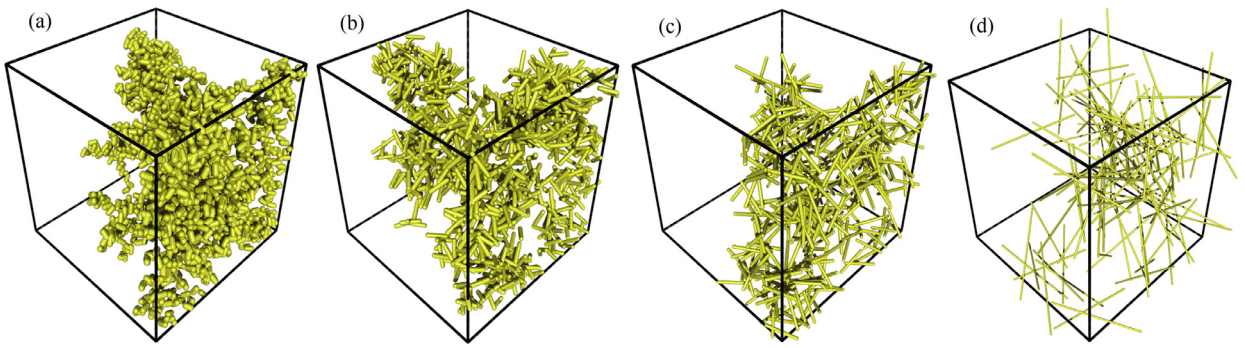

Fig. 3. Visualizations of percolating clusters in the two-phase porous materials shown in Fig. 2:(a) $\alpha=1$, (b) $\alpha=4$, (c) $\alpha=10$, and (d) $\alpha=50$.

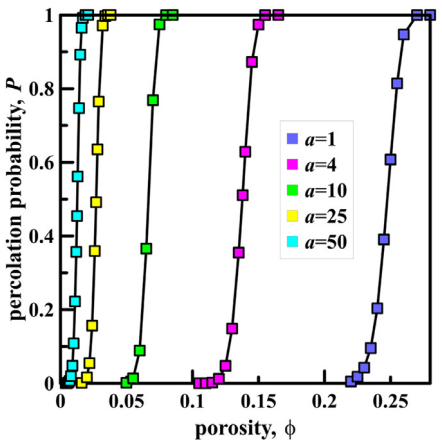

Fig. 4. The curves of P-ϕ in the finite system of $L=50$. The symbols and solid lines are simulated and fitting data, respectively.

percolating clusters in the spherocylindrical porous systems shown in Fig. 2, where α is the aspect ratio defined as $\alpha=H/D$, where H is the height of cylinder part and D is the diameter of its semi-spherical cap. Plus, as an introductory example, Fig. 4 shows the curves of P-ϕ in the finite system of $L=50$ for spherocylindrical porous systems of various α.

From Fig. 4, one can see that P increases with ϕ, and the P–ϕ curves shift to lower porosities, with unchanged slope, for spherocylindrical pores. This indicates that the curve slope is strongly dependent on the porosity, rather than the shape. Nevertheless, the position of P–ϕ curve is primarily determined by the pore shape. Based on the above numerical strategy, we can simulate different P–ϕ curves in various L and α, and correspondingly approximate $\phi_c(L)$ and $\Delta(L)$ by the error function, then eventually obtain ϕ_c of different α by Eq. (3). Herein, we directly present the numerical results of ϕ_c for different α and employ the famous excluded-volume theory (Balberg et al., 1985; Xu et al., 2016b) to fit these numerical

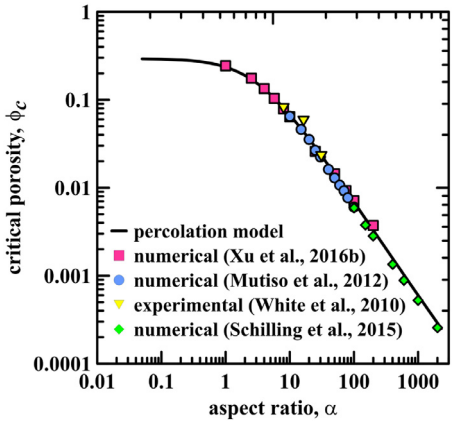

Fig. 5. The excluded-volume percolation model for ϕ_c versus the numerical and experimental data of the percolation threshold of overlapping spherocylindrical objects.

results, as shown in Fig. 5. Eq. (4) gives the excluded-volume percolation model of interpenetrating spherocylindrical porous networks. Fig. 5 also displays the comparisons of the present percolation model with the numerical and experimental data reported in literature (Mutisoet al., 2012; Schilling et al., 2015; White et al., 2010; Xu et al., 2016b). It is clearly shown that the excluded-volume percolation model for ϕ_c is in excellent agreement with the numerical and experimental data over a wide range of α. These comparisons suggest that the excluded-volume percolation model can accurately determine the global percolation threshold with arbitrary aspect ratio. Therefore, we reasonably expect that the precise percolation model can be applied to good predictions of the tortuosity and transport properties of porous materials.

$$\phi_c = 1 - \exp\left\{-\left[1 + (0.14\alpha + 0.17)^{-0.32}\right]/V_{dex}\right\} \tag{4}$$

where V_{dex} is the dimensionless excluded volume defined as the ratio of the excluded volume V_{ex} to the volume V of spherocylinder, that is

$$V_{dex} = \frac{V_{ex}}{V} = 2 + \frac{6(1+\alpha)(1+0.5\alpha)}{(1+1.5\alpha)} \tag{5}$$

3. Continuum percolation-based tortuosity model (CPTM)

In this section, we investigate the geometrical tortuosity in the framework of the continuum percolation theory. In general, porous structures possess a fractal configuration, specifically a fractal path consisting of steps of length Δx. Several researchers (Falconer, 1985; Wheatcraft & Tyler, 1988) have proposed the total length $L(\Delta x)$ of fractal path in relation to the fractal dimensionality D_f of porous networks, that is

$$L(\Delta x) = L^{D_f} \Delta x^{1-D_f} \tag{6}$$

where the fractal dimensionality D_f is a space-dependent quantity reflecting the scaling of the most probable fluid flow path, e.g., $D_f = 1.21$ in 2D and $D_f = 1.43$ in 3D (Sheppard, Knackstedt, Pinczewski, & Sahimi, 1999). Following the recent works (Ghanbarian et al., 2013; Hunt & Sahimi, 2017) in lattice percolation, the step lengths tend to zero when the percolation of porous networks occurs, so that each step length Δx is inversely proportional to the correlation length ξ, namely, $\Delta x \propto 1/\xi$, owing to the divergency nature of ξ near the percolation threshold. Thus, Eq. (6) is rewritten as

$$L(\xi) \propto L^{D_f} \xi^{D_f - 1} \tag{7}$$

where $L(\xi)$ exactly illustrates the actual length of fluid flow path in fractal porous networks, since ξ is the mean distance between any two sites on the same cluster. According to Eqs. (1),(2) and (7), the geometrical tortuosity should satisfy the following scaling relation in lattice percolation (Hunt & Sahimi, 2017).

$$\tau \propto |p - p_c|^{\nu - \nu D_f} \tag{8}$$

Whereas such the scaling relation cannot reflect the effect of pore shape. Accordingly, we have to map the lattice percolation to the continuum percolation by replacing p and p_c with ϕ and ϕ_c. Note that p is essentially the number density not the volume fraction. The inter-transformation between ϕ and p is strongly dependent on the pore-size distribution (PSD). For the scaling relation of Eq. (8), the PSD effect can be implied in the pre-factor of Eq. (8). Consequently, a scaling expression for the continuum percolation-based geometrical tortuosity is presented by

$$\tau \propto |\phi - \phi_c|^{\nu - \nu D_f} \tag{9}$$

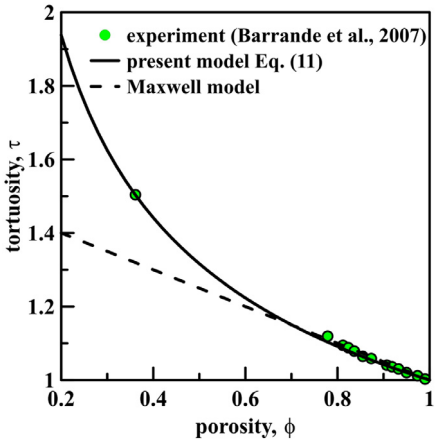

Fig. 6. Comparisons of the predicted tortuosity τ from CPTM and Maxwell model proposed in the literature (Barrande et al., 2007) with the experimental data of electrical tortuosity of spherical glass beads (Barrande et al., 2007). Spherocylindrical pore space of $\alpha = 20$ and $L = 100$ is selected, resulting in the critical porosity is $\phi_c = 0.0359$ through Eq. (4).

Eq. (9) is valid for the infinite-size system. Also, the effect of pore shape is reflected by the critical porosity ϕ_c, as depicted in Eq. (4). However, in practice, the size of material structures (or samples) is often finite, and the size-dependence of various properties cannot be ignored in numerical simulations and experimental studies. Hence, it is necessary to invoke finite-size scaling into Eq. (9) to extend the applicable range of CPTM. Here, we adopt the finite-size scaling operated by Xu et al. (2018a), (2018e) who set $\xi = L$ and generated a finite-size scaling factor $(C/L)^{1/\nu}$ (see Eq. (2)). Consequently, we incorporate the finite-size scaling factor into our continuum percolation-based tortuosity scaling relation, and yield

$$\tau \propto \left|\phi - \phi_c + (C/L)^{1/\nu}\right|^{\nu - \nu D_f} \tag{10}$$

From Eq. (10), one can see when the porosity is close to the percolation threshold (i.e., $\phi = \phi_c$), the present relation portrays the size-dependence of tortuosity in a power-law manner. On the other hand, if $\phi \to 1$, meaning that a two-phase porous material reduces to the sole porous phase, namely, $\tau = 1$, which generates a scale coefficient of $|1 - \phi_c + (C/L)^{1/\nu}|^{\nu Df - \nu}$ for Eq. (10). Therefore, the continuum percolation-based tortuosity model (CPTM) can be explicitly expressed as

$$\tau = \left|\frac{1 - \phi_c + (C/L)^{1/\nu}}{\phi - \phi_c + (C/L)^{1/\nu}}\right|^{\nu D_f - \nu} \tag{11}$$

Invoking the percolation threshold model presented in the preceding section (see Eq. (4)), the critical correlation length exponent of $\nu = 0.88$ in 3D, the fractal dimensionality of $D_f = 1.43$ and the coefficient of $C = 0.85$, CPTM (Eq. (11)) can address the dependence of geometrical tortuosity on the pore shape. It is worth mentioning that the sample size L is normally large enough compared to the coefficient C, which leads to the value of C/L ($C/L << 1$) is only a little contribution to the determination of tortuosity.

To test the CPTM, we compare the predicted tortuosity τ from the present CPTM with extensive experimental and numerical results from various porous materials reported in literature (Barrande, Bouchet, & Denoyel, 2007; Iwai, Shikazono, & Matsui, 2010; Tomadakis & Sotirchos, 1993). Fig. 6 presents the comparisons of the predicted τ from CPTM and Maxwell model ($\tau = 1.5 - 0.5\phi$, see Eq. (8) in the literature (Barrande et al., 2007)) with the experimental data of electrical tortuosity of spherical glass beads with the mean size of 30 μm (Barrande et al., 2007). It can be clearly seen that the predicted τ from CPTM is in so excellent agreement with the experimental data, which implies the accuracy of CPTM is favorable. With respect to the experimental data, the Maxwell model can estimate precisely τ at a high porosity (e.g., $\phi > 0.65$) but no longer valid at a low porosity. It is not surprisingly that the Maxwell theory is supposed to be valid for diluted particle fraction (corresponding to the high porosity). Also, the linear variation from the Maxwell model cannot illustrate the tortuosity near the percolation threshold, as shown in Fig. 6. In addition, the experimental results of diffusive tortuosity of Solid Oxide Fuel Cells (SOFC) porous electrodes reported by Iwai et al. (2010) are also used to compare with the theoretical values of τ from the present CPTM, as shown in Fig. 7. The agreement is good in the whole range of porosities, specifically near the percolation threshold.

On the other hand, Fig. 8 shows a comparison of CPTM with numerical simulations on the tortuosity of 3D random fiber structures (Tomadakis & Sotirchos, 1993). One can see that the predicted values are basically consistent with the numerical results under different porosities. Through these extensive comparisons depicted in Figs 6–8, it is adequately confirmed that the proposed CPTM is capable of reliably predicting the tortuosity of porous networks in various porous materials, especially near the percolation threshold and above. Additionally, in views of Figs 6–8, they all show that the tortuosity deceases with increasing porosity in a power-law manner, and the attenuation amplitude is striking near the critical porosity. It implies that the pore shape has a significant impact on the geometrical tortuosity, which will be discussed in Section 5.

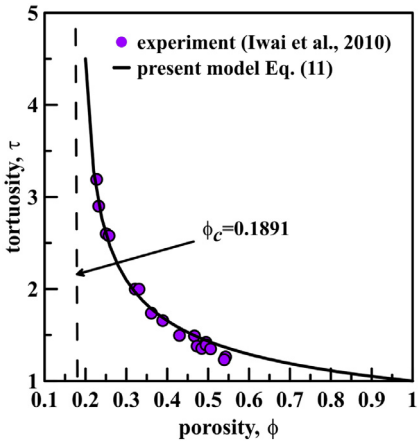

Fig. 7. Comparison of the predicted τ from CPTM with the experimental data of diffusive tortuosity of SOFC porous electrodes (Iwai et al., 2010). Spherocylindrical pore space of $\alpha = 2$ and $L = 100$ is selected, resulting in the critical porosity is $\phi_c = 0.1891$ through Eq. (4).

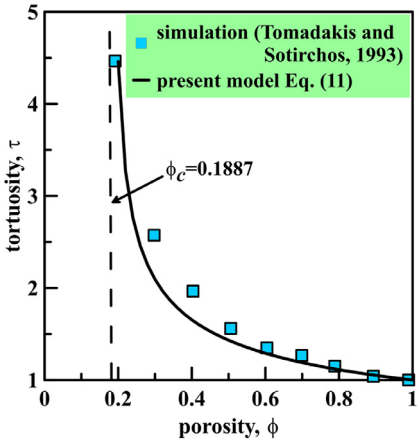

Fig. 8. Comparison of the predicted τ from CPTM with the numerical results of diffusive tortuosity of 3D random fiber structures (Tomadakis & Sotirchos, 1993). Spherocylindrical pore space of $\alpha = 2.01$ and $L = 100$ is selected, resulting in the critical porosity is $\phi_c = 0.1887$ through Eq. (4).

4. Continuum percolation-based generalized effective medium theory (CP-GEMT)

The problems for the prediction of various effective transport parameters like the conductivity, permeability, permittivity and diffusivity of porous materials are mathematically analogous. These transport parameters can transform each other through the classical Nernst–Einstein relation (Weinert & Mason, 1980). Without loss of generality, the effective diffusivity of porous materials is here considered as the description purpose.

In the present two-phase porous materials, we assume the porosity and diffusivity of pore space to be ϕ and D_p, and that of homogeneous matrix to be (1-ϕ) and D_m. According to the effective medium approximation and percolation theory, the diffusivity of two-phase materials in relation to the percolation threshold has been proposed by (McLachlan, Blaszkiewicz, & Newnham, 1990)

$$\frac{D_{eff}}{D_p} = \left(\frac{\phi - \phi_c}{1 - \phi_c}\right)^t \text{for} \phi > \phi_c, \text{and} \frac{D_{eff}}{D_m} = \left(1 - \frac{\phi}{\phi_c}\right)^{-t} \text{for} \phi < \phi_c \tag{12}$$

where D_{eff} is the effective diffusivity of two-phase materials, t is the transport-percolation exponent whose universal value is 2 in 3D lattice percolation (1.43 in 2D) (Stauffer & Aharony, 2003). But it is found to might be a nonuniversal value in continuum percolation that decreases substantially with the increasing aspect ratio of 3D oblong objects ($t \leq 2$) (Foygel, Morris, Anez, French, & Sobolev, 2005). Recently, the exponent t is also expected to be larger than 2 ($t > 2$) in complex geometries of pore space (Ghanbarian & Daigle, 2016; Oh & Jiang, 2004; Xu et al., 2018a). For Eq. (12), a drawback is that it cannot evaluate the diffusivity near the percolation threshold, as the effective diffusivity $D_{eff} \to 0$ or ∞ at $\phi = \phi_c$ (see the following Fig. 9).

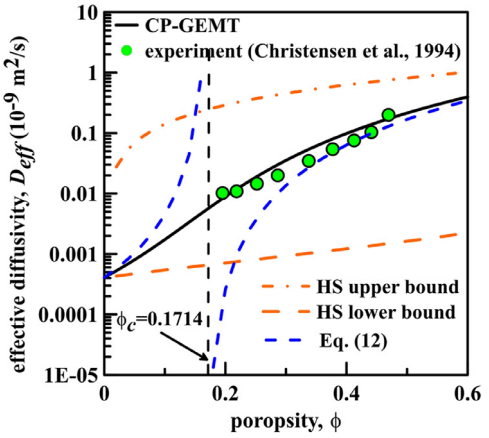

Fig. 9. Comparisons of the predicted D_{eff} from CP-GEMT, Eq. (12) and HS bounds (Eq. (19)) with the experimental data of diffusivity of ordinary cement paste (Christensen et al., 1994). Spherocylindrical pore space of $\alpha = 2.5$ results in the critical porosity of $\phi_c = 0.1714$. The selection of other parameters (e.g., $t = 2.7$ and $D_m/D_p = 2\text{E-}04$) follows the experiment.

Alternatively, Kirkpatrick (1973) presented an effective conductivity model containing the percolation threshold by using the average field theory, which can be written as the form of diffusivity:

$$\phi\frac{\left(D_p - D_{eff}\right)}{D_p + (0.5Z-1)D_{eff}} + (1-\phi)\frac{\left(D_m - D_{eff}\right)}{D_m + (0.5Z-1)D_{eff}} = 0 \tag{13}$$

where Z is the average coordination number. Although $0.5Z$ is a good approximation on the percolation threshold in 2D case, it not a good prediction of the percolation threshold in 3D by Sahimi (2003) and the references therein.

Accordingly, to overcome these shortcomings, McLachlan (1987) proposed a generalized effective medium theory (GEMT, see Eq. (14)) to link the effective transport properties of two-phase composite media to the critical porosity by using Bruggeman's symmetric and asymmetric theories. As stated by McLachlan (1987), GEMT is valid at all porosities, of which detailed formulations have been illustrated by McLachlan (1987). We directly present GEMT as follows:

$$\frac{f_L\left(D_L^{1/t} - D_{eff}^{1/t}\right)}{D_L^{1/t} + [(1-\phi_c)/\phi_c]D_{eff}^{1/t}} + \frac{(1-f_L)\left(D_H^{1/t} - D_{eff}^{1/t}\right)}{D_H^{1/t} + [(1-\phi_c)/\phi_c]D_{eff}^{1/t}} = 0 \tag{14}$$

where f_L and D_L are the volume fraction and diffusivity of low-diffusion components, respectively. D_H is the diffusivity of high-diffusion components. By further combining the percolation threshold illustrated in Section 2 and GEMT, a continuum percolation-based generalized effective medium theory (CP-GEMT) can be developed to predict the effective diffusivity of porous materials, as depicted in Eq. (15). Also, the CP-GEMT can address the effect of pore shape on the effective transport properties.

$$\frac{f_L\left(D_L^{1/t} - D_{eff}^{1/t}\right)}{D_L^{1/t} + \left[e^{F(\alpha)}/\left(1-e^{F(\alpha)}\right)\right]D_{eff}^{1/t}} + \frac{(1-f_L)\left(D_H^{1/t} - D_{eff}^{1/t}\right)}{D_H^{1/t} + \left[e^{F(\alpha)}/\left(1-e^{F(\alpha)}\right)\right]D_{eff}^{1/t}} = 0 \tag{15}$$

where $F(\alpha)$ is a function on the aspect ratio α of spherocylindrical pores, according to Eqs. (4) and (5), $F(\alpha)$ is written as

$$F(\alpha) = -(1+1.5\alpha)\left[\frac{1+(0.14\alpha+0.17)^{-0.32}}{2(1+1.5\alpha)+6(1+\alpha)(1+0.5\alpha)}\right] \tag{16}$$

when pores are considered as high-diffusion components, namely, $D_H = D_p$ and $\phi = 1\text{-}f_L$; whilst the homogeneous solid matrix is regarded as low-diffusion components, namely, $D_L = D_m$. In contrast, if pores are low-diffusion components, namely, $D_L = D_p$, $f_L = \phi$, and $D_H = D_m$. Thus, the normalized effective diffusivity of porous materials is formulated by

$$\frac{D_{eff}}{D_m} = \left[\Omega + \sqrt{\Omega^2 + \frac{\left(1-e^{F(\alpha)}\right)}{e^{F(\alpha)}}\left(\frac{D_p}{D_m}\right)^{1/t}}\right]^t \tag{17}$$

with

$$\Omega = \frac{1}{2e^{F(\alpha)}}\left[e^{F(\alpha)} - \phi + \left(\phi + e^{F(\alpha)} - 1\right)\left(\frac{D_p}{D_m}\right)^{1/t}\right] \tag{18}$$

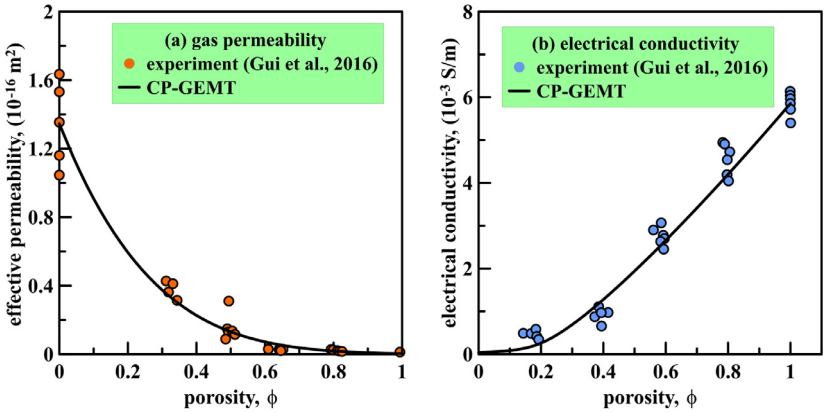

Fig. 10. Comparisons of the predicted gas permeability and electrical conductivity with the experimental measurements of normal concrete (Gui et al., 2016). The aspect ratio of pores is prescribed to be $\alpha = 2$ followed by the experiment recently reported by Chen et al. (2017). (a) $t = 4.5$ (Oh & Jiang, 2004) and $C_m = 1.34522\text{E-}016$ m^2 (Gui et al., 2016); (b) $t = 1.2$ (Foygel et al., 2005) and $C_p = 5.8543\text{E-}03$ S/m (Gui et al., 2016).

The CP-GEMT reduces to Eq. (12) for $\phi > \phi_c$ when $D_p \,/\, D_m = 0$. Note that the CP-GEMT Eqs. (17) and ((18)) is not only suitable for predicting the diffusion problem of porous media, but can allow the predictions of electrical/thermal/magnetic conductivity, permeability and permittivity of two-phase porous materials through the Nernst–Einstein relation (Weinert & Mason, 1980), namely, $D_p \,/\, D_m = C_p \,/\, C_m$ and $D_{eff} \,/\, D_m = C_{eff} \,/\, C_m$, where C_{eff} is the effective conductivity (permeability, or permittivity), C_p and C_m are the conductivities (permeabilities, or permittivities) of pores and matrix, respectively. In what follows, we will verify the reliability of the proposed CP-GEMT.

We first utilize CP-GEMT to compute the effective diffusivity of two-phase porous media and compare the derived theoretical results with the experimental data of chloride diffusivity of ordinary cement paste (Christensen et al., 1994) that is usually considered as a two-phase material composed of bulk paste of low-diffusion phase and capillary pores of high-diffusion phase (D_p is the chloride diffusivity in free water, e.g., $D_p = 2.032\text{E-}09$ m^2/s (Christensen et al., 1994)), as shown in Fig. 9. Moreover, we also compare the present CP-GEMT with Eq. (12) and the well-known Hashin–Shtrikman (HS) bounds (Hashin & Shtrikman, 1962) (see the following Eq. (19)). Good agreement is presented for the comparison of CP-GEMT with the experimental data of diffusivity. Also, the present CP-GEMT is rigorously within the scope of the HS bounds. As illustrated above, Fig. 9 obviously shows the failure of Eq. (12) near the percolation threshold. All of these indicate that the proposed CP-GEMT can predict well the diffusivity of porous materials over the whole range of porosities. It is worth mentioning that the selection of $\alpha = 2.5$ of spherocylindrical pore space that generates the good agreement also validates the recent experimental studies on the examination of pore shape (e.g., $\alpha = 2.5$ (Sun & Scherer, 2010) and 2 (Chen, Li, Ruan, Sagoe-Crentsil, & Duan, 2017)) in cement-based materials. Furthermore, the derived critical porosity of $\phi_c = 0.1714$ is very close to the previous investigation on the percolation threshold of capillary pores (e.g., $\phi_c = 0.17$ (Bentz, Jensen, Coats, & Glasser, 2000)) in cement-based materials.

$$D_{eff} = \begin{cases} D_L + \dfrac{1-f_L}{\frac{1}{D_H - D_L} + \frac{f_L}{3D_L}}, \text{lowerbound} \\ D_H + \dfrac{f_L}{\frac{1}{D_L - D_H} + \frac{1-f_L}{3D_H}}, \text{upperbound} \end{cases} \tag{19}$$

Subsequently, we use CP-GEMT to predict respectively the gas permeability and electrical conductivity of porous materials and compare with the experimental measurements recently studied by Gui, Qin, and Li (2016), as shown in Fig. 10. As expected, Fig. 10(a) shows that the predicted values of gas permeability reasonably match measurements. Also, a power-variation of the gas permeability with porosity is manifested due to the effect of percolation of porous networks. It is noted that pores are regarded as non-permeable components as they are fully filled with liquid in that experiment, in other words, the gas permeability of pores is prescribed to be zero. Consequently, the gas permeability nonlinearly decays with the increase of porosity, as shown in Fig. 10(a). Herein, the percolation exponent is set to be $t = 4.5$ followed the study presented by Oh and Jiang (2004). Similarly, Fig. 10(b) also presents that the predicted values of electrical conductivity are in good line with the experimental results. Nevertheless, the electrical conductivity monotonously increases with the porosity contrast to the gas permeability, as shown in Fig. 10(b), since the fact that the pores filled with liquid is an intrinsic conductor and cement paste is here considered as the insulator even if it is exactly a weak conductor. In addition, unlike the distinct power-variation shown in Fig. 10(a), Fig. 10(b) displays a slight power-relation of the electrical conductivity to the porosity. This attributes to the transport-percolation exponent close to unity, namely, $t = 1.2$, of which the selection follows the electrical conductivity study of carbon nanotube composites (t is in the range between 1.2 and 1.6) (Foygel et al., 2005). It suggests that the transport-percolation exponent t plays a significant role in the curve shape of transport parameter-porosity, which will be discussed in the following section. Irrespective of these interesting findings, it can be validated from Fig. 10 that

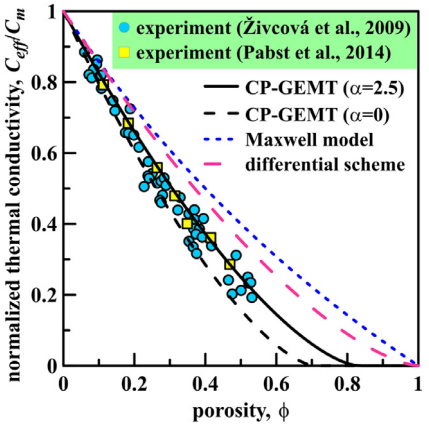

Fig. 11. Comparisons of the predicted values of normalized effective thermal conductivity from CP-GEMT, Maxwell model and differential effective scheme with the experimental data from porous alumina ceramics (Živcová et al., 2009) and porous zirconia ceramics (Pabst & Gregorová, 2014). The transport-percolation exponent is prescribed to be $t = 1.5$.

the proposed CP-GEMT meets the expectation of the experimental studies on gas permeability and electrical conductivity of porous materials over the whole range of porosities.

Moreover, the available experimental data of thermal conductivity from porous ceramics of two types (Pabst & Gregorová, 2014; Živcová et al., 2009) is used as a benchmark comparison against those predicted values derived by different theoretical models like the present CP-GEMT, Maxwell model (see the following Eq. (20) (Xu et al., 2014, 2018a, 2018d)) and differential effective scheme (Eq. (21) (Xu et al., 2018b)), as shown in Fig. 11. As described by Pabst and Gregorová (2014), pores are viewed as perfectly insulating inclusions so that the conductivity of pores is negligible in both porous ceramics. Consequently, Fig. 11 shows the attenuation tendency of the thermal conductivity with the porosity from these theoretical predictions and the experimental results. Also, one can see that, with respect to the experimental data, the prediction of CP-GEMT is more accurate than that of differential effective scheme and Maxwell model, especially for CP-GEMT with $\alpha = 2.5$, as shown in Fig. 11. We find the results from CP-GEMT with $\alpha = 2.5$ are obviously larger than that from CP-GEMT with $\alpha = 0$. In terms of the definition of α illustrated in Section 2, spherocylindrical pores of $\alpha = 0$ virtually degenerate to isotropic spherical pores. It means that isotropic pores underestimate the thermal conductivity of porous ceramics. Therefore, the shape effect of pores should be considered in theoretical and numerical studies on the physico-mechanical properties of porous materials, which will be described in the following section. On the other hand, the differential scheme also displays a power relation of the thermal conductivity to the porosity that is therefore closer to the experimental data than the Maxwell model, but both theoretical models cannot accurately predict the thermal conductivity, especially in a high porosity (see Fig. 11), since both effective medium approximations rely on the knowledge of the effective property in the dilute limit of inclusion fraction (Torquato, 2002). Note that the expressions of Maxwell model (Eq. (20)) and differential scheme (Eq. (21)) adopted here are both based on the case of spherical inclusions. Through these comparisons displayed in Figs. 9–11, we deeply believe that the proposed CP-GEMT can well predict various effective transport properties of porous media in the entire range of porosities and not only near the percolation threshold.

$$\frac{D_{eff}}{D_m} = \frac{2D_m + D_p + 2\phi(D_p - D_m)}{2D_m + D_p - \phi(D_p - D_m)}, \text{ for Maxwell model} \tag{20}$$

$$1 - \phi = \left(\frac{D_m}{D_{eff}}\right)^{\frac{1}{3}} \left(\frac{D_{eff} - D_p}{D_m - D_p}\right), \text{ for differential effecitve scheme} \tag{21}$$

5. Results and discussion

5.1. Effect of pore shape on tortuosity

Fig. 12 presents the effect of aspect ratio of spherocylindrical pores on the geometrical tortuosity of two-phase porous materials, by using the present CPTM. One can clearly see that, under a constant porosity, the tortuosity τ decays with the increase of aspect ratio α in a power-law manner, and the attenuation amplitude is strongly dependent on porosity ϕ. The variation scheme is very similar to the relation of tortuosity to porosity shown in Figs 6–8. Actually, the amplitude dependence is subjected to the synergetic effect between aspect ratio and porosity, since the percolation threshold is controlled by the aspect ratio. When ϕ tends to ϕ_c induced by α, τ is divergent according to Eq. (11), where C/L is set to be zero. As such, the divergence configuration does not appear in $\phi = 0.3$ and 0.4, as shown in Fig. 12. This is because the maximum

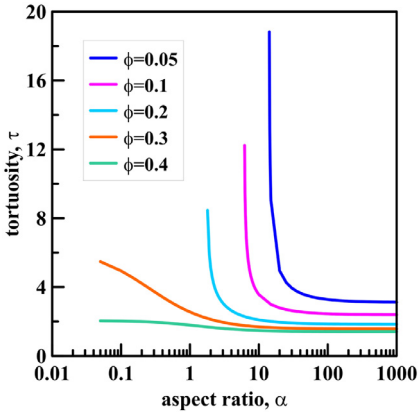

Fig. 12. Effect of spherocylindrical pore shape on the geometrical tortuosity under different porosities. C/L is set to be zero.

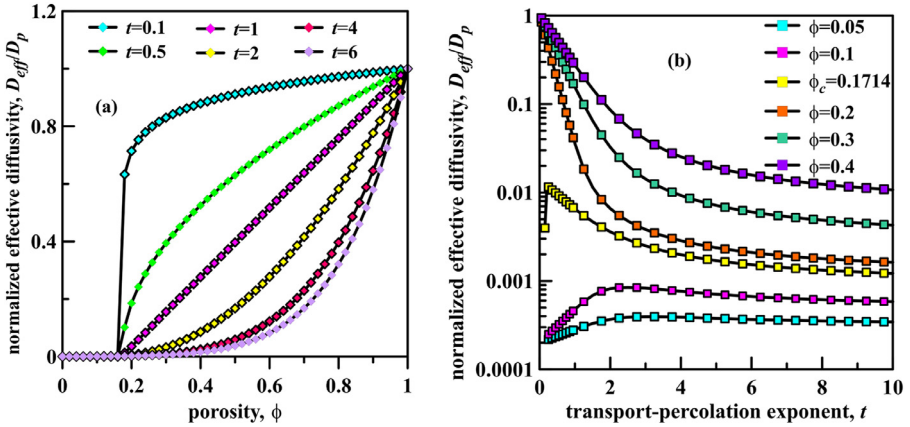

Fig. 13. Coupled effects of porosity ϕ and transport-percolation exponent t on the normalized effective diffusivity D_{eff}/D_p. The selection of other parameters follows that depicted in Fig. 9, such as $\alpha = 2.5$ and $D_m/D_p = 2E\text{-}04$.

percolation threshold for spherocylindrical pores is less than 0.3, to be specific, the maximum percolation threshold corresponds to the percolation threshold of spherical pores, namely, $\phi_c = 0.29$, as shown Fig. 5. The present results confirm that the power-law dominates the tortuosity of porous materials near the percolation threshold. More importantly, the present results shed light on the pore shape dependence in the power-law manner.

5.2. Coupled effects of porosity and transport-percolation exponent on the effective diffusivity

We analyze the sensitivity of the proposed CP-GEMT to porosity ϕ and transport-percolation exponent t, as shown in Fig. 13. The two-phase porous material is here regarded as ordinary cement paste depicted in Fig. 9 and the normalized effective diffusivity D_{eff}/D_p is investigated. Fig. 13(a) illustrates the variation of D_{eff}/D_p with ϕ under different t. Each curve of D_{eff}/D_p-ϕ is divided into two stages: the stable-germination stage and the power-growth stage, by the individual inflection point denoted as ϕ_{in}. In the stable-germination stage, D_{eff}/D_p slowly increases or holds steady with ϕ, depending on the value of t. Whereas in the power-growth stage, D_{eff}/D_p increases with ϕ in a power-law manner. In addition, Fig. 13(a) shows that the emergence of inflection point strongly depends on t. To be specific, the large t generates the high ϕ_{in}. It is worth stressing that ϕ_{in} may be greater/less than or equal to ϕ_c. For instance, for $t = 4$, $\phi_{in} \approx 0.3 > \phi_c = 0.1714$ ($\alpha = 2.5$); for $t = 0.1$, $\phi_{in} = 0.1715 \approx \phi_c = 0.1714$. Although Fig. 13(a) presents that the results of ϕ_{in} are always larger than or equal to ϕ_c, the case of $\phi_{in} < \phi_c$ can be found in Fig. 10(b), where $\phi_{in} \approx 0.1 < \phi_c = 0.1891$ ($\alpha = 2$). It is of significance for our results to validate that the method for deriving the percolation threshold through empirical analysis the curve of property-porosity is failure, which derives essentially the inflection point ϕ_{in}, rather than the percolation threshold ϕ_c. Plus, t controls the curve shape in the second stage. When $t < 1$, the second stage shape is convex, and the convexity increases with the reduction of t. When $t = 1$, the second stage shape is linear, due to the power-law degenerates to the linear relation according to Eqs. (17) and (18). The concave shape of the second stage occurs in $t > 1$, and the concavity rapidly increases as t deviates from 1 then flat-increases with the large t, like the tendency of D_{eff}/D_p with t shown in Fig. 13(b).

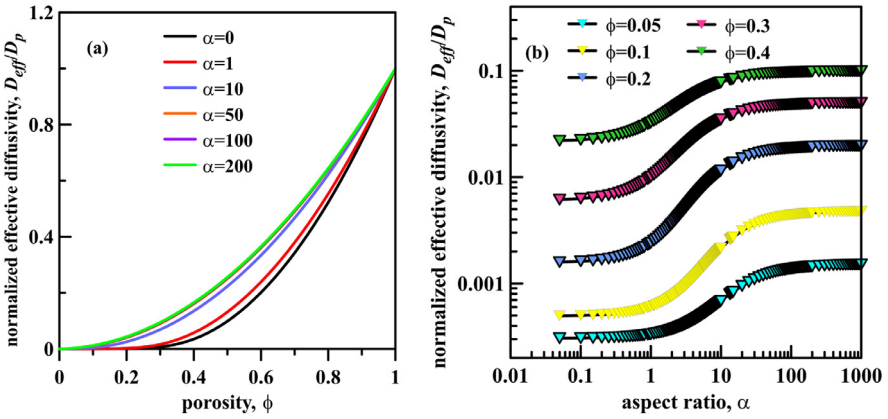

Fig. 14. (a) Effect of porosity ϕ on the normalized effective diffusivity D_{eff}/D_p under different aspect ratios α; (b) Effect of α on D_{eff}/D_p under different ϕ. The selection of other parameters follows that depicted in Fig. 9.

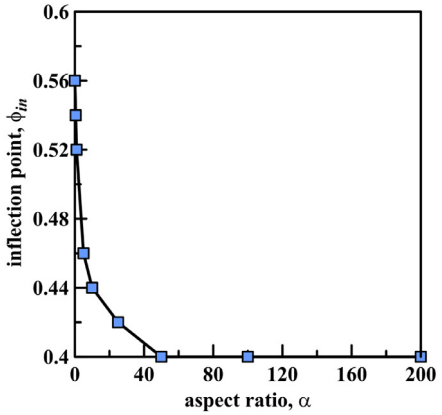

Fig. 15. Effect of α on the inflection point ϕ_{in} of D_{eff}/D_p-ϕ curve presented in Fig. 14(a).

On the other hand, Fig. 13(b) presents the effect of t on D_{eff}/D_p under different ϕ. Our results show that the percolation threshold has an important effect on the curve of D_{eff}/D_p-t. Strictly speaking, when $\phi \le \phi_c$, D_{eff}/D_p first increases and then decreases with t, and the inflection point of t gradually reduces as ϕ increases from 0 to the percolation threshold. However, the curve of D_{eff}/D_p-t is a monotonical power-attenuation function as $\phi > \phi_c$, as shown in Fig. 13(b). It appears to be the first time to our knowledge that such interesting phenomena are presented.

5.3. Effect of pore shape on the effective diffusivity

We further investigate the sensitivity of the proposed CP-GEMT to the pore shape characterized by the spherocylindrical aspect ratio α, as shown in Fig. 14. Actually, the effect of α can also be mapped to the effect of percolation threshold ϕ_c on the normalized effective diffusivity D_{eff}/D_p, on the basis of Eq. (4) and Fig. 5. Fig. 14(a) presents the curves of D_{eff}/D_p-ϕ under different α. One can see that these curve shapes are concave independent of the variation of α, consistent with that of $t > 1$ shown in Fig. 13(a). It indicates that the curve of D_{eff}/D_p-ϕ is more sensitive to the transport-percolation exponent t than to the aspect ratio α. However, α regulates the inflection point ϕ_{in} of D_{eff}/D_p-ϕ curve, especially in the smaller α, ϕ_{in} monotonically decreases as α increases from 0 to 50, and then gets to a constant value of 0.4 with the continuous increase of α, as shown in Fig. 15. This is one reason why the curves of D_{eff}/D_p-ϕ for $\alpha = 50$, 100 and 200 almost coincide, as depicted in Fig. 14(a). Moreover, the value of D_{eff}/D_p dramatically relies on α, as show in Fig. 14(b). Our results show that D_{eff}/D_p satisfies a "*S*-shaped" increment scheme with the increase of α under a fixed ϕ. Interestingly, when $\alpha = 0$, meaning that spherocylindrical pores degenerate to spherical pores, D_{eff}/D_p has the minimal value. This illustrates anisotropic-shaped pores giving rise to the increment of effective diffusivity. It is so surprised that the present find is contrary to the theoretical investigations in previous researches (Li, Zeng, & Xu, 2017; Markov et al., 2013; Pabst & Gregorová, 2014) that spherical pores would have the maximal conductivity in two-phase spheroidal pore systems. The present conclusion does not mean to bear in mind that the proposed CP-GEMT would be failure. In contrast, such a conclusion instead confirms a significant issue that the accurate percolation threshold of porous networks possessing a prominent effect on the transport properties is a

universal decreasing monotonic function on α, and the maximal percolation threshold emerges in $\alpha = 0$, as shown in Fig. 5. Indeed, the percolation threshold of porous networks is larger; the interconnectivity potential of pores is more difficult, so that the power-variation of transport properties expectedly delays under a specific porosity ϕ and transport-percolation exponent t. As shown in Fig. 15, the inflection point ϕ_{in} is the maximal value when $\alpha = 0$. However, in those previous studies (Li et al., 2017; Markov et al., 2013; Pabst & Gregorová, 2014), the percolation of pores was not considered, and pores were regarded as rigid inclusions with non-diffusing (or insulating) configuration. Effective medium theories including the differential effective scheme (Markov et al., 2013), self-consistent model (Pabst & Gregorová, 2014) and Mori–Tanaka approximation (Li et al., 2017) were utilized to evaluate the effective conductivity of spheroidal inclusion systems. The limitations of these effective medium theories have been illustrated in Introduction section.

6. Conclusions

Accurate theoretical formalism provides an important tool for virtual material testing and design, in order to efficiently and thoroughly understand the influences of various key design/control variables for rapid material prototyping and manufacturing. This strategy will avoid unnecessary costs, reducing trial-and-error campaigns and lead to fast material developments with tailored properties and desirable performance. In this paper, we have systematically presented a generic theoretical framework to accurately predict the percolation threshold and tortuosity of anisotropic-shaped porous networks and a diversity of effective transport properties including diffusivity, gas permeability, electrical and thermal conductivity of two-phase porous materials. In particular, three powerful continuum percolation-based models were respectively devised to determine these important structural and physical parameters of porous materials, including a coupled scheme of Monte Carlo simulations and the excluded-volume percolation model, a continuum percolation-based tortuosity model (CPTM) and a continuum percolation-based generalized effective medium theory (CP-GEMT). The three proposed models can lead to explicit and general procedures readily applicable to other complex networks composed of arbitrary overlapping discrete objects such as cracks, particles, interfaces and capsules, though the present work has taken 3D spherocylindrical porous networks as a focus. In fact, the model of spherocylindrical pores can also be of interest as an “asymptotic model” for carbon nanotubes, nanowires and fibers and as an “equivalent model” for other deviations from the percolation threshold of porous networks.

By comparing with extensive experimental and numerical data on the percolation threshold and tortuosity of various porous materials, the former two models have been validated to be efficient tools for the accurate estimations of the percolation threshold and tortuosity of porous networks, respectively. Furthermore, comparisons against experimental measurements of transport properties (e.g., diffusivity, gas permeability, electrical and thermal conductivity) of different porous materials and predicted results from other theoretical models indicated that the proposed CP-GEMT is capable of predicting a variety of transport properties of porous materials over the entire range of porosities ϕ to a very high accuracy. Moreover, we showed quantitatively how the pore configurations (e.g., pore shape and porosity) dominate the tortuosity and transport properties of porous materials. The results revealed a power-law dependence of the tortuosity on the porosity ϕ and aspect ratio α of spherocylindrical pore space, specifically near the percolation threshold ϕ_c. Although the normalized effective diffusivity D_{eff}/D_p has also a power-law scaling with ϕ, the curves of D_{eff}/D_p-ϕ strongly depend on the non-universal value of transport-percolation exponent t. Also, t and α control the emergence of inflection point ϕ_{in} of D_{eff}/D_p-ϕ curve. It is very important that ϕ_{in} is not ϕ_c, which can be greater/less than or equal to ϕ_c. This sheds light on the failure of previous methods for obtaining the percolation threshold through empirical analysis the curves of effective properties-porosity reported in literature, which derived essentially the inflection point ϕ_{in}, rather than the percolation threshold ϕ_c. In addition, we found that the normalized effective diffusivity D_{eff}/D_p is monotonic increasing function of the aspect ratio α and obtained a quantitative functional form. Last but not least, we elucidated that anisotropic-shaped pores can lead to the increase of effective diffusivity, which differs distinctly from the previous studies for spheroidal inclusion systems reported in the literature.

Acknowledgments

This work was supported by the National Key Research and Development Program of China [grant number: 2017YFC0404902]; the National Natural Science Foundation of China [grant number 11772120]; the Natural Science Foundation of Jiangsu Province [grant number BK20170096]; and the Fundamental Research Funds for the Central Universities [grant number 2016B06314]. The State Scholarship Fund from China Scholarship Council is also acknowledged.

References

Araújo, N., Grassberger, P., Kahng, B., Schrenk, K. J., & Ziff, R. M. (2014). Recent advances and open challenges in percolation. *The European Physical Journal Special Topics, 223*(11), 2307–2321.

Balberg, I., Binenbaum, N., & Wagner, N. (1984). Percolation thresholds in the three-dimensional sticks system. *Physical Review Letters, 52*(17), 1465–1468.

Barrande, M., Bouchet, R., & Denoyel, R. (2007). Tortuosity of porous particles. *Analytical Chemistry, 79*(23), 9115–9121.

Bentz, D. P., Jensen, O. M., Coats, A. M., & Glasser, F. P. (2000). Influence of silica fume on diffusivity in cement-based materials, I. Experimental and computer modeling studies on cement pastes. *Cement and Concrete Research, 30*(6), 953–962.

Beran, M. J. (1968). *Statistical continuum theories*. New York: Wiley.

Broadbent, S. R., & Hammersley, J. M. (1957). Percolation processes: I. Crystals and mazes. *Mathematical Proceedings of the Cambridge Philosophical Society, 53*(3), 629–641.

Brosseau, C. (2002). Generalized effective medium theory and dielectric relaxation in particle-filled polymeric resins. *Journal of Applied Physics, 91*(5), 3197–3204.
Chen, S. J., Li, W. G., Ruan, C. K., Sagoe-Crentsil, K., & Duan, W. H. (2017). Pore shape analysis using centrifuge driven metal intrusion: Indication on porosimetry equations, hydration and packing. *Construction and Building Materials, 154*, 95–104.
Christensen, B. J., Coverdale, R. T., Olson, R. A., Ford, S. J., Garboczi, E. J., Jennings, H. M., et al. (1994). Impedance spectroscopy of hydrating cement-based materials: Measurement, interpretation and application. *Journal of the American Ceramic Society, 77*(11), 2789–2804.
Clennell, M. B. (1997). Tortuosity: A guide through the maze. In M. A. Lovell, & P. K. Harvey (Eds.), *Developments in petrophysics* (pp. 299–344). London: Geological Society Special Publication. No. 122.
Diamond, S. (2000). Mercury porosimetry: An inappropriate method for the measurement of pore size distributions in cement-based materials. *Cement and Concrete Research, 30*(10), 1517–1525.
Falconer, K. J. (1985). *The geometry of fractal sets*. Cambridge: Cambridge University Press.
Foygel, M., Morris, R. D., Anez, D., French, S., & Sobolev, V. L. (2005). Theoretical and computational studies of carbon nanotube composites and suspensions: Electrical and thermal conductivity. *Physical Review B, 71*(10), 104201.
Ghanbarian, B., & Daigle, H. (2016). Thermal conductivity in porous media: Percolation-based effective-medium approximation. *Water Resources Research, 52*, 295–314.
Ghanbarian, B., Hunt, A. G., Sahimi, M., Ewing, R. P., & Skinner, T. E. (2013). Percolation theory generates a physically based description of tortuosity in saturated and unsaturated porous media. *Soil Science Society of America Journal, 77*(6), 1920–1929.
Giraud, A., Nguyen, N. B., & Grgic, D. (2012). Effective poroelastic coefficients of isotropic oolitic rocks with micro and meso porosities. *International Journal of Engineering Science, 58*(6), 57–77.
Gui, Q., Qin, M., & Li, K. (2016). Gas permeability and electrical conductivity of structural concretes: Impact of pore structure and pore saturation. *Cement and Concrete Research, 89*, 109–119.
Hashin, Z., & Shtrikman, S. (1962). A variational approach to the theory of the effective magnetic permeability of multiphase materials. *Journal of Applied Physics, 33*(10), 3125–3131.
Hermann, H., & Elsner, A. (2014). Geometric models for isotropic random porous media: A review. *Advances in Materials Science & Engineering, 562874*, 1–16.
Hunt, A. G. (2004). Continuum percolation theory and Archie's law. *Geophysical Research Letters, 31*(19), L19503.
Hunt, A. G., & Sahimi, M. (2017). Flow, transport, and reaction in porous media: Percolation scaling, critical-path analysis, and effective medium approximation. *Reviews of Geophysics, 55*, 993–1078.
Isichenko, M. B. (1992). Percolation, statistical topography, and transport in random media. *Review of Modern Physics, 64*(4), 961–1043.
Iwai, H., Shikazono, N., Matsui, T., Teshima, H., Kishimoto, M., Kishida, R., et al. (2010). Quantification of SOFC anode microstructure based on dual beam FIB–SEM technique. *Journal of Power Sources, 195*(4), 955–961.
Kapitulnik, A., Aharony, A., Deutscher, G., & Stauffer, D. (1983). Self-similarity and correlations in percolation. *Journal of Physics A, 16*(8), L269–L274.
Kirkpatrick, S. (1973). Percolation and conduction. *Review of Modern Physics, 45*(4), 574–588.
Li, H., Zeng, Q., & Xu, S. (2017). Effect of pore shape on the thermal conductivity of partially saturated cement-based porous composites. *Cement and Concrete Composites, 81*, 87–96.
Lin, J., Chen, H., & Xu, W. X. (2018). Geometrical percolation threshold of congruent cuboidlike particles in overlapping particle systems. *Physical Review E, 98*(1), 012134.
Markov, M., Mousatov, A., Kazatchenko, E., & Markova, I. (2013). Electrical conductivity of percolating two-component rock-like materials. *Journal of Physics D, 46*(15), 155301.
McLachlan, D. S. (1987). An equation for the conductivity of binary mixtures with anisotropic structures. *Journal of Physics C, 20*(7), 865–877.
McLachlan, D. S., Blaszkiewicz, M., & Newnham, R. E. (1990). Electrical resistivity of composites. *Journal of the American Ceramic Society, 73*(8), 2187–2203.
Mutiso, R. M., Sherrott, M. C., Li, J., & Winey, K. I. (2012). Simulations and generalized model of the effect of filler size dispersity on electrical percolation in rod networks. *Physical Review B, 86*(21), 214306.
Nan, C.-W., Shen, Y., & Ma, J. (2010). Physical properties of composites near percolation. *Annual Review of Materials Research, 40*(1), 131–151.
Oh, B. Y., & Jiang, S. Y. (2004). Prediction of diffusivity of concrete based on simple analytic equations. *Cement and Concrete Research, 34*(3), 463–480.
Pabst, W., & Gregorová, E. (2014). Conductivity of porous materials with spheroidal pores. *Journal of European Ceramic Society, 34*(11), 2757–2766.
Rintoul, M. D., & Torquato, S. (1997). Precise determination of the critical threshold and exponents in a three-dimensional continuum percolation model. *Journal of Physics A, 30*(16), L585–L592.
Sahimi, M. (2003). *Heterogeneous materials I: Linear transport and optical properties*. Berlin: Springer-Verlag.
Schilling, T., Miller, M. A., & van der Schoot, P. (2015). Percolation in suspensions of hard nanoparticles: From spheres to needles. *EPL, 111*, 56004.
Sevostianov, I., Chen, F., Giraud, A., & Grgic, D. (2016). Compliance and resistivity contribution tensors of axisymmetric concave pores. *International Journal of Engineering Science, 101*, 14–28.
Sevostianov, I., & Giraud, A. (2013). Generalization of Maxwell homogenization scheme for elastic material containing inhomogeneities of diverse shape. *International Journal of Engineering Science, 64*, 23–36.
Sevostianov, I., & Shrestha, M. (2010). Cross-property connections between overall electric conductivity and fluid permeability of a random porous media with conducting skeleton. *International Journal of Engineering Science, 48*(12), 1702–1708.
Sevostianov, I., Trofimov, A., Merodio, J., Penta, R., & Rodriguez-Ramos, R. (2017). Connection between electrical conductivity and diffusion coefficient of a conductive porous material filled with electrolyte. *International Journal of Engineering Science, 121*, 108–117.
Sevostianova, E., Leinauer, B., & Sevostianov, I. (2010). Quantitative characterization of the microstructure of a porous material in the context of tortuosity. *International Journal of Engineering Science, 48*(12), 1693–1701.
Sheppard, A. P., Knackstedt, M. A., Pinczewski, W. V., & Sahimi, M. (1999). Invasion percolation: New algorithm and university classes. *Journal of Physics A, 32*(49), L521–L529.
Stauffer, D., & Aharony, A. (2003). *Introduction to percolation theory* (2nd revised ed). London: Taylor & Francis.
Sun, Zh., & Scherer, G. W. (2010). Pore size and shape in mortar by thermoporometry. *Cement and Concrete Research, 40*(5), 740–751.
Suvorov, A. P., & Selvadurai, A. P. S. (2011). Effective medium methods and a computational approach for estimating geomaterial properties of porous materials with randomly oriented ellipsoidal pores. *Computers & Geotechnics, 38*(5), 721–730.
Tang, X. W., Sun, Z. F., & Cheng, G. C. (2012). Simulation of the relationship between porosity and tortuosity in porous media with cubic particles. *Chinese Physics B, 21*(10), 100201.
Tomadakis, M. M., & Sotirchos, S. V. (1993). Ordinary and transition regime diffusion in random fiber structures. *AIChE Journal, 39*(3), 397–412.
Torquato, S. (2002). *Random heterogeneous materials: Microstructure and macroscopic properties*. New York: Springer-Verlag.
Torquato, S., & Jiao, Y. (2012). Effect of dimensionality on the continuum percolation of overlapping hyperspheres and hypercubes. *The Journal of Chemical Physics, 137*(7), 074106.
Torquato, S., & Jiao, Y. (2013). Effect of dimensionality on the percolation threshold of overlapping nonspherical hyperparticles. *Physical Review E, 87*(2), 022111.
Torquato, S., & Pham, D. C. (2004). Optimal bounds on the trapping constant and permeability of porous media. *Physical Review Letters, 92*, 255505.
Trofimov, A., Abaimov, S. G., Akhatov, I., & Sevostianov, I. (2018a). On the bounds of applicability of two-step homogenization technique for porous materials. *International Journal of Engineering Science, 123*, 117–126.
Trofimov, A., Markov, A., Abaimov, S. G., Akhatov, I., & Sevostianov, I. (2018b). Overall elastic properties of a material containing inhomogeneities of concave shape. *International Journal of Engineering Science, 132*, 30–44.
Weinert, U., & Mason, E. A. (1980). Generalized Nernst–Einstein relations for nonlinear transport coefficients. *Physical Review A, 21*(2), 681–690.

Wheatcraft, S. W., & Tyler, S. W. (1988). An explanation of scale-dependent dispersivity in heterogeneous aquifers using concepts of fractal geometry. *Water Resources Research, 24*(4), 566–578.
White, S. I., Mutiso, R. M., Vora, P. M., Jahnke, D., Hsu, S., Kikkawa, J. M., et al. (2010). Electrical percolation behavior in silver nanowire-polystyrene composites: Simulation and experiment. *Advanced Functional Materials, 20*(16), 2709–2716.
Winslow, D. N., Cohen, M. D., Bentz, D. P., Snyder, K. A., & Garboczi, E. J. (1994). Percolation and pore structure in mortars and concrete. *Cement and Concrete Research, 24*(1), 25–37.
Xu, W. X., Chen, H. S., Chen, W., & Jiang, L. H. (2014). Prediction of transport behaviors of particulate composites considering microstructures of soft interfacial layers around ellipsoidal aggregate particles. *Soft Matter, 10*(4), 627–638.
Xu, W. X., Jia, M. K., & Gong, Z. (2018a). Thermal conductivity and tortuosity of porous composites considering percolation of porous network: From spherical to polyhedral pores. *Composites Science and Technology, 167*, 134–140.
Xu, W. X., Jia, M. K., Zhu, Z. G., Liu, M., Lei, D., & Gou, X. F. (2018b). *n*-Phase micromechanical framework for the conductivity and elastic modulus of particulate composites: Design to microencapsulated phase change materials (MPCMs)-cementitious composites. *Materials and Design, 145*, 108–115.
Xu, W. X., Ma, H. F., Ji, S., & Chen, H. (2016a). Analytical effective elastic properties of particulate composites with soft interfaces around anisotropic particles. *Composites Science and Technology, 129*, 10–18.
Xu, W. X., Su, X., & Jiao, Y. (2016b). Continuum percolation of congruent overlapping spherocylinders. *Physical Review E, 94*(3), 032122.
Xu, W. X., Sun, H., Chen, W., & Chen, H. (2018c). Transport properties of concrete-like granular materials interacted by their microstructures and particle components. *International Journal of Modern Physics B, 32*(18), 1840011.
Xu, W. X., Wu, F., Jiao, Y., & Liu, M. (2017a). A general micromechanical framework of effective moduli for the design of nonspherical nano- and micro-particle reinforced composites with interface properties. *Materials and Design, 127*, 162–172.
Xu, W. X., Wu, Y., & Jia, M. K. (2018d). Elastic dependence of particle-reinforced composites on anisotropic particle geometries and reinforced/weak interphase microstructures at nano- and micro-scales. *Composite Structures, 203*, 124–131.
Xu, W. X., Xu, B., & Guo, F. (2017b). Elastic properties of particle-reinforced composites containing nonspherical particles of high packing density and interphase: DEM-FEM simulation and micromechanical theory. *Computer Methods in Applied Mechanics and Engineering, 326*, 122–143.
Xu, W. X., Zhu, Z. G., & Zhang, D. (2018e). Continuum percolation-based tortuosity and thermal conductivity of soft superball systems: Shape dependence from octahedra via spheres to cubes. *Soft Matter*. doi:10.1039/C8SM01488D.
Xu, X. F. (2012). Ellipsoidal bounds and percolation thresholds of transport properties of composites. *Acta Mechanica, 223*(4), 765–774.
Yun, M. J., Yu, B. M., Zhang, B., & Huang, M. T. (2005). A geometry model for tortuosity of streamtubes in porous media with spherical particles. *Chinese Physics Letters, 22*(6), 1464–1467.
Yun, M. J., Yue, Y., Yu, B. M., Lu, J. D., & Zheng, W. (2010). A geometry model for tortuosity of tortuous streamlines in porous media with cylindrical particles. *Chinese Physics Letters, 27*(10), 104704.
Živcová, Z., Gregorová, E., Pabst, W., Smith, D. S., Michot, A., & Poulier, C. (2009). Thermal conductivity of porous alumina ceramics prepared using starch as a pore-forming agent. *Journal of the European Ceramic Society, 29*(3), 347–353.